# MODELLING THE NON-ADIABATIC BLOWDOWN OF PRESSURISED CRYOGENIC HYDROGEN STORAGE TANK

**Cirrone, D.[1], Makarov, D.[1], Kashkarov, S.[1], Friedrich, A.[2], Molkov, V.[1]**
**[1]HySAFER Centre, Ulster University, Newtownabbey, Northern Ireland, BT37 0QB, UK,**
**[2]Karlsruhe Institute of Technology, Eggenstein-Leopoldshafen, 76344, Germany,**
**d.cirrone@ulster.ac.uk, dv.makarov@ulster.ac.uk, s.kashkarov@ulster.ac.uk,**
**v.molkov@ulster.ac.uk, andreas.friedrich@kit.edu**

## ABSTRACT

This paper describes a model of hydrogen blowdown dynamics for storage tanks needed for hydrogen safety engineering to accurately represent incident scenarios. Heat transfer through a tank wall affects the temperature and pressure dynamics inside the storage vessel, and therefore the characteristics of the resulting hydrogen jet in case of loss of containment. Available non-adiabatic blowdown models are validated only against experiments on hydrogen storages at ambient temperature. Effect of heat transfer for cryo-compressed hydrogen can be more significant due to a larger temperature difference between the stored hydrogen and surrounding atmosphere, especially in case of failure of equipment insulation. Previous work by the authors demonstrated that the heat transfer through a discharge pipe wall can significantly affect the mass flow rate of cryogenic hydrogen releases. To the authors' knowledge thoroughly validated models of non-adiabatic blowdown dynamics for cryo-compressed hydrogen are currently missing. The present work further develops the non-adiabatic blowdown model at ambient temperature using the under-expanded jet theory developed at Ulster University, to expand it to cryo-compressed hydrogen storages. The non-ideal behaviour of cryo-compressed hydrogen is accounted through the high-accuracy Helmholtz energy formulations. The developed model includes effect of heat transfer at both the tank and discharge pipe wall. The model is thoroughly validated against sixteen tests performed by Pro-Science on blowdown of hydrogen storage tanks with initial pressure 0.5-20 MPa and temperature 80-310 K, through release nozzle of diameter 0.5-4.0 mm. The model well reproduces the experimental pressure and temperature dynamics during the entire blowdown duration.

**Keywords**: cryogenic hydrogen, non-adiabatic blowdown, conjugate heat transfer, physical model, hydrogen safety engineering

## 1. INTRODUCTION

The fast-growing market of hydrogen technologies requires competitive techniques to store and transport large quantities of this energy carrier. The cryo-compressed hydrogen (CcH2) storage is being investigated as it may optimise the gravimetric and volumetric capacities against the energy required for the compression and cooling down of the gas in comparison to commercially used compressed gaseous (CGH2) and liquid hydrogen ($LH_2$) [1,2]. Furthermore, storage of cryo-compressed hydrogen is not affected by the boil-off as LH2 storage. Studies [3–5] investigated the refuelling of storage systems with hydrogen at 80 K and pressures up to 35 MPa for light duty vehicles. The inherently safer design of CcH2 storage systems and refuelling infrastructure requires an understanding of potential incident consequences. In case of a release through the Thermally Activated Pressure Relief Device (TPRD) or other relief device installed on a storage system, the hydrogen blowdown dynamics and transient mass transfer will be affected by the heat transfer in the system. This, in turn, would influence hydrogen parameters at the release nozzle, and, consequently, the hazard distances of unignited and ignited jets. During blowdown of pressurised hydrogen system, temperature in a storage tank decreases due to the gas expansion. This process competes with the tendency of the gas temperature to increase due to the heat transfer through the tank wall from the surrounding atmosphere to hydrogen. In 2007 Schefer et al. [6] highlighted the importance of heat transfer in the storage tank blowdown dynamics. This effect should be even more pronounced in the case of CcH2 storage tanks with damaged insulation. Several experimental and analytical studies have assessed the effect of heat transfer during filling of high-pressure hydrogen storage tanks at initial ambient temperature [7],[8],[9]. In 2019, Molkov et al. [10] developed and validated a physical model against experiments on fuelling of hydrogen storage tanks with volume in the range 29-74 L and pressures up to 77 MPa. The model accuracy was within

temperature deviations measured during experiments. Fewer studies have been conducted on the modelling of non-adiabatic blowdown of hydrogen storage tanks. In 2021, Molkov et al. [11] developed a physical model accounting for heat transfer through the wall of high pressure hydrogen tanks in an engulfing fire while releasing hydrogen through a TPRD. This model employed the under-expanded jet theory developed earlier by Molkov et al. [12] to calculate parameters at the real and notional nozzle exits. The model was validated against experimental data on the blowdown of 19 L, 70 MPa Type IV tank with 1 mm TPRD orifice filled in by helium, and the destructive fire test with 36 L, 70 MPa Type IV hydrogen tank. While the Abel-Noble EoS was proved to represent well conditions and blowdown dynamics of high-pressure hydrogen storage tanks at initial ambient temperature [11], it may have limited applicability to cryogenic hydrogen gas. In this case, the high-accuracy Helmholtz energy formulations, e.g. by Leachman et al. [13], are generally employed for the EoS, as implemented by the National Institute of Standards and Technology (NIST). In the previous works of authors [14,15] it was shown that the deviation in calculated conditions at the release nozzle and dispersion between Abel-Noble EoS and NIST EoS becomes significant for storage pressure higher than 0.6 MPa and grows with the increase of pressure. Thus, NIST EoS shall be used for calculations. Furthermore, the heat transfer through the wall of a release pipe connecting the storage system to the nozzle may affect the cryogenic flow characteristics, as proved in the numerical study carried out by Cirrone et al. in 2022 [16]. In 2021, Venetsanos et al. [17] developed a simplified 1D transient model to account for the discharge line effects, i.e. pressure losses and heat transfer, during blowdown of ambient and cryogenic hydrogen storages. However, the experimentally measured time history of temperature and pressure in the storage tank were used as an input to the model, preventing validation of the combined non-adiabatic blowdown and discharge line modelling, and its application for arbitrary initial conditions of the hydrogen storage. No validated models are available to accurately represent the blowdown dynamics of CcH2 tanks. The present study proposes a new physical model expanding the work [11]. In the proposed formulation, the non-ideal behaviour of CcH2 is taken into account by implementing the EoS with high-accuracy Helmholtz energy formulations [13] and properties from CoolProp open source database [18]. The non-adiabatic blowdown model accounts for the heat transfer through the storage tank and discharge pipe walls by solving an unsteady 1D heat transfer equation. The model performance is assessed through comparison with experimental measurements of temperature and pressure during blowdown of hydrogen storage tanks at initial ambient and cryogenic (80 K) temperature. Sixteen experimental tests performed within PRESLHY project [19,20], with initial storage pressure in the range 0.6-20.0 MPa abs and release diameter in the range 0.5-4.0 mm, were used for the model validation.

## 2. VALIDATION EXPERIMENTS

Tests performed on the DISCHA facility by Pro-Science within the PRESLHY project [19,20] were used here for the validation of developed non-adiabatic blowdown model. The tank was made of stainless-steel and had volume $V$=2.81 L. The cylindrical tank had internal diameter $D_{int}$=160 mm and internal height of 140 mm. Wall thickness ($L_t$) was 30 mm at the top and bottom of the tank, whereas it was 20 mm at the vertical wall. The tank was exposed to ambient air for the ambient temperature release tests (Figure 1a). For the cryogenic release tests, the tank was placed in a cooling box and immerged in a liquid nitrogen ($LN_2$) bath with temperature equal to 77 K (Figure *1*b). Figure 1c shows a scheme of the experimental facility and equipment for the cryogenic tests. The hydrogen release line (overall system) was located at height of 30 mm from the tank bottom. The release line included a tubular connection (kept as short as possible) between the tank and the release valve, which were immerged into the $LN_2$ bath. This was followed by the discharge pipe, exposed to ambient air for both ambient and cryogenic temperature tests, ending into a circular nozzle. This pipe had length equal to 55 mm, internal and external diameters equal to 10 and 12 mm respectively. Four nozzles with circular apertures of diameter equal to 0.5, 1.0, 2.0 and 4.0 mm were used in the experiments. A static pressure sensor was used to measure the pressure inside the tank during the release test. Two sets of thermocouples were installed inside the tank at different heights to capture the temperature behaviour during the tests. The first set included three closed standard type K thermocouples with a sensitive tip covered by thin stainless-steel shell (indicated as TC1, TC2, TC3). The second set included three open thermocouples where the stainless-steel shell of the sensitive tip was removed (indicated as TC1o, TC2o and TC3o). Both sets were installed in comparable positions inside the vessel. Two further closed thermocouples

were placed in the discharge line: one sensor was placed into the hydrogen flow after the release valve (TC4) and another sensor was inserted into the stainless-steel material at the nozzle ($TC_{nz}$). More details on the experimental set-up and equipment are available in [19,20].

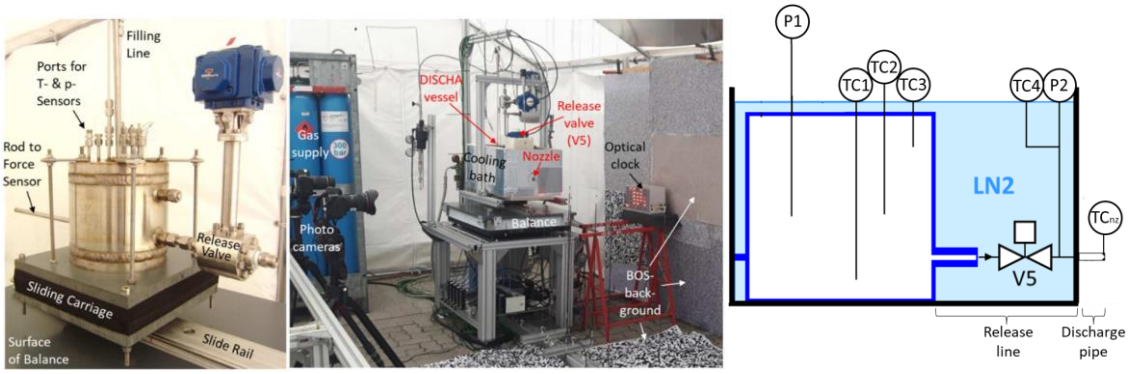


(a) (b) (c)

Figure 1. The DISCHA facility for ambient (a) and cryogenic (b) temperature tests including the $LN_2$ bath cooling box and additional equipment; scheme of the DISCHA facility for cryogenic tests (c) [20].

Sixteen tests were selected to maximize the validation domain of the model. They cover initial storage pressure $P_s$=0.6-20 MPa abs, initial storage temperature $T_s$ =80-310 K, release nozzle diameter $d_n$=0.5-4.0 mm. Table 1 shows the initial storage conditions and nozzle diameter for each test. $T_s$ in Table 1 is the average of the three closed thermocouples readings (TC1-TC3) prior to the blowdown start.

Table 1. Parameters (nozzle diameter, pressure and temperature) of the sixteen validation tests.

| **Cryogenic temperature releases** | | | | **Ambient temperature releases** | | | |
|---|---|---|---|---|---|---|---|
| Test No. | $d_n$, mm | $P_s$, MPa abs | $T_s$, K | Test No. | $d_n$, mm | $P_s$, MPa abs | $T_s$, K |
| 1c | 0.5 | 0.59 | 83.7 | 1w | 0.5 | 0.59 | 310.4 |
| 4c | 0.5 | 20.12 | 80.2 | 4w | 0.5 | 20.19 | 310.4 |
| 5c | 1 | 0.61 | 86.0 | 5w | 1 | 0.62 | 305.9 |
| 8c | 1 | 20.1 | 84.8 | 8w | 1 | 20.19 | 307.7 |
| 9c | 2 | 0.6 | 81.2 | 9w | 2 | 0.69 | 302.3 |
| 15c | 2 | 20.25 | 81.5 | 15w | 2 | 20.22 | 310.3 |
| 16c | 4 | 0.61 | 80.2 | 16w | 4 | 0.59 | 296.0 |
| 22c | 4 | 20.27 | 80.2 | 22w | 4 | 20.03 | 300.9 |

## 3. PHYSICAL MODEL DESCRIPTION

The present physical model advances the non-adiabatic blowdown model accounting for heat transfer through the wall of high pressure hydrogen storage tanks developed in [11,21] to extend its applicability to CcH2 releases and to account for the heat transfer through the discharge line. The novelties of the methodology presented in this work compared to models [11,21] will be highlighted in the description. The developed model accounts for the non-ideal behaviour of hydrogen at high pressure and cryogenic temperature through the EoS based on high-accuracy Helmholtz energy formulations [13], instead of the Abel-Noble EoS as in [11,21], implemented via the opensource CoolProp C++ library [18]. CoolProp allows to calculate hydrogen properties by knowing two variables of its thermodynamic state. The first law of thermodynamics is used to assess the change of storage conditions during blowdown. Figure 2a shows the scheme of a tank wall and the parameters affecting the heat transfer. The rate of the hydrogen internal energy, $U$, change in the tank is calculated from the rate of heat transfer, $Q$, to/from hydrogen through the tank wall and the rate of enthalpy of the hydrogen outflow, $h_{out}$, [11]:

$$\frac{dU}{dt} = \frac{dQ}{dt} - h_{out}\frac{dm}{dt}\,. \tag{1}$$

In Eq. (1), the rate of heat transfer by convection at the internal wall is calculated as [11]:

$$\frac{dQ}{dt} = k_{int} A_{int} \left(T_{w(int)} - T_1\right), \quad (2)$$

where $A_{int}$ is the internal area of the tank, $T_{w(int)}$ is the temperature of the internal tank wall, $T_1$ is the temperature of hydrogen in the tank, $k_{int}$ is the heat transfer coefficient at the internal wall (Eq. (3)).

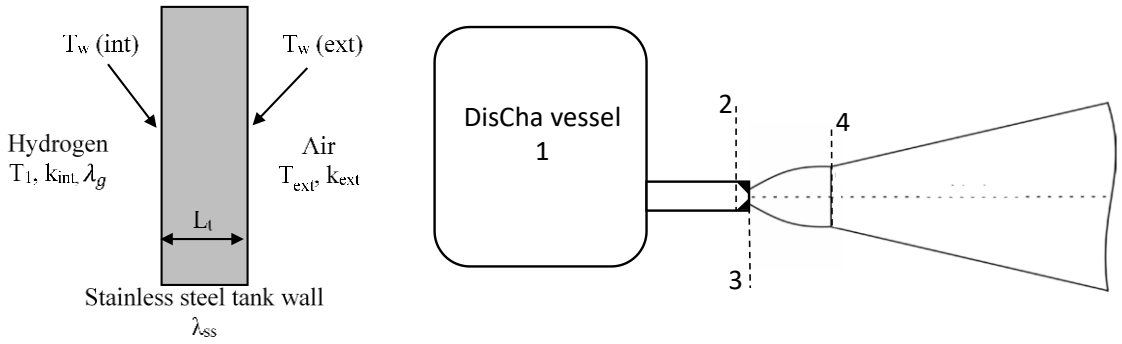


(a) (b)

Figure 2. a) Scheme of a tank wall and parameters used in the conjugate heat transfer calculations. b) Schematic of the model: 1 – storage tank with tabular connection to valve under LN2 temperature; 1-2 – discharge pipe under atmospheric temperature; 2 – end of pipe prior to the nozzle; 2-3 – real nozzle; 3 – real nozzle exit; 3-4 – notional nozzle; 4 - notional nozzle exit.

The considered tank and release system are schematically shown in Fig. 2b. The under-expanded jet theory [12] calculates hydrogen parameters in the storage tank (location "1" in Fig. 2b), and flow conditions at the exit (location "3") of the real nozzle ("2-3") and at the exit (location "4") of the notional nozzle ("3-4") during the tank blowdown. In the validation tests hydrogen is released from the tank into atmosphere through a release system and discharge pipe (see Fig. 1c). The connection between the tank and the valve in Fig. 1c was kept as short as possible and all these components were immerged into the $LN_2$ bath for the cryogenic tests. The heat exchange area for this release line is significantly smaller than the surface of the storage tank placed in the same $LN_2$ bath. Thus, it is considered that the heat exchange through the release line immerged in the $LN_2$ bath can be neglected. After the valve, hydrogen flows through the discharge pipe ("1-2") exposed to ambient air, and thus subject to strong heat transfer that cannot be neglected especially for cryogenic tests. Thus, the under-expanded jet theory [12] cannot be applied in a straight forward way and must be expanded to account for the heat transfer through the discharge pipe and non-ideal gas behaviour by the NIST EoS based on high-accuracy Helmholtz energy formulations [13]. More details are provided in Sections 3.2 and 3.3 respectively.

### 3.1. Convective and conductive heat transfer for the storage tank

The convective heat transfer inside the tank and within the discharge pipe is calculated according to the convection regime: natural, forced or combined. The regime is defined by the ratio of the Grashof to Reynolds number to determine the corresponding Nusselt number, $Nu$, following the methodology [11]. The convective heat transfer coefficient at the internal tank wall is then calculated as [10]:

$$k_{int} = \frac{\lambda_g \times Nu}{D_{int}}. \quad (3)$$

The full set of equations to assess the convective heat transfer at internal tank wall are given in [10]. $\lambda_g$ is the thermal conductivity of the gas, which is provided by CoolProp database (Section 3.4 for details). The model solves the unsteady heat conduction equation through a tank wall exposed on one side to hydrogen at temperature $T_1$ and on another side to the surrounding air at ambient temperature $T_{ext}$, as shown in Figure 2a. The 1D heat conduction equation is applied [22], and the boundary conditions at internal and external surfaces of the tank are defined as in [11] where the full set of equations is given.

### 3.2. Heat transfer through the discharge line wall

CoolProp library [18] implementing the NIST EoS [13] allows to calculate the thermodynamic state and properties of hydrogen by knowing two parameters of a single-phase fluid. For each time *t* during

calculations, $P_1$ and $T_1$ are used to calculate density, enthalpy and entropy, respectively $\rho_1$, $h_1$, $s_1$. If the discharge pipe between storage tank and nozzle is not insulated, heat transfer through the pipe wall may strongly affect the flow parameters at the real nozzle exit. The developed model takes into account the heat transfer through the release pipe wall (see Fig. 2b). Due to the presence of a nozzle of smaller diameter at the pipe end downstream, it is assumed that $P_2 = P_1$. The first and the second law of thermodynamics are combined to assess the effect of heat transfer on the fluid properties:

$$dh = Q + vdp. \tag{4}$$

The heat transfer through the discharge pipe wall is calculated at each time step *t* as:

$$\frac{dQ}{dt} = k_{int,pipe} A_{int,pipe} \left(T_{w,pipe(int)} - T_1\right). \tag{5}$$

Here $k_{int,pipe}$ is the convective heat transfer coefficient calculated for either forced, combined, or natural convection [11]; $A_{int,pipe}$ is the internal surface of the pipe; and $T_{w,pipe(int)}$ is the temperature at the pipe wall surface interfacing the hydrogen, which is calculated by the 1D heat conduction equation. For the present case, it will also be considered the assumption of $T_{w,pipe(int)}$ as constant in time, without solving the 1D heat conduction equation through the pipe wall, to simplify the model and speed up calculations. $T_1$ is the temperature of hydrogen in the storage tank, as it is assumed to be equal to that of the flow at the entrance of the pipe exposed at the outer surface to air at ambient temperature. The validity of this assumption for the investigated cryo-compressed releases is supported by the experimental evidence. Finally, it is possible to use the energy conservation equation to retrieve the thermodynamic state $h_2$ at the end of the pipe, prior to enter the nozzle section:

$$h_2 + \frac{v_2^2}{2} = q + h_1, \tag{6}$$

with velocity, $v_2$, and specific heat transfer, *q*, calculated as:

$$v_2 = \dot{m}_3/(A_{int}\rho_2) \text{ and } q = \frac{\frac{dQ}{dt}}{\dot{m}_3} \text{ [23].} \tag{7}$$

The transient values of hydrogen mass flow rate $\dot{m}_3$ and hydrogen density at the pipe exit from the previous time step are used to solve Eq. (7). Value of $h_2$ are calculated from Eq. (6). Afterwards, this parameter is used as input to CoolProp database along with pressure $P_2 = P_1$ to estimate the remaining parameters of the hydrogen flow at the end of pipe prior to enter the nozzle section: $T_2, s_2$ and $\rho_2$.

### 3.3. Under-expanded jet theory with inclusion of NIST EoS

The under-expanded jet theory in [12] is expanded to take into account the heat transfer through the discharge pipe and non-ideal gas behaviour through the NIST EoS [13]. Hydrogen flows through the pipe in conditions of heat transfer from the surroundings. Then, due to short length of the nozzle at the end of pipe, we assume that hydrogen undergoes isentropic expansion in the short real nozzle, i.e. $s_2 = s_3$. The flow is choked at the real nozzle exit, i.e. the velocity is equal to local speed of sound. The energy conservation equation is employed to calculate conditions at the real nozzle exit and is solved using an iterative algorithm:

$$h_3^n - h_2 + \frac{(v_3^n)^2}{2} - \frac{{v_2}^2}{2} = \Delta^n. \tag{8}$$

Temperature decreases gradually by $\Delta T$ along the isentropic transformation from the conditions at location 2 to 3, i.e. $s_3^n(T, P) = s_2(T_2, P_2)$. For each iteration *n*, the enthalpy, $h_3^n(T_3^n, s_3 = s_2)$, and the speed of sound, $u_3^n(T_3^n, s_3 = s_2)$, at the real nozzle exit are determined by the CoolProp database by using the condition $s_3 = s_2$ and $T_3^n$, i.e. temperature at the iteration *n*. The algorithm stops when the equation of energy conservation is satisfied with a given tolerance, Δ (see Section 3.4). Temperature $T_3^{end}$, providing the satisfaction of Eq. (8) is the jet temperature at the real nozzle exit. Knowing $T_3$ and $s_3$, it is possible to determine from the CoolProp database all other properties of interest, i.e. $v_3$, $P_3$ and $\rho_3$. The mass flow rate is calculated as $\dot{m}_3 = \rho_3 v_3 A_3$. In the case of the discharge pipe absence or if the pipe is properly vacuum insulated, the model can be amended to evaluate direct expansion from the storage to the nozzle and skip steps described in Section 3.2. The expansion of the flow in the notional nozzle from location "3" (real nozzle exit) to ambient pressure ($P_4 = P_{amb}$) at location "4" (notional nozzle exit) assumes the conservation of energy and speed of sound at the notional nozzle exit:

$$h_3 + \frac{{v_3}^2}{2} = h_4 + \frac{{v_4}^2}{2}. \quad (9)$$

The equation is solved using an iterative algorithm as per Eq. (8) by changing $T_4$ by a given $\Delta T$ and use CoolProp to calculate the parameters in Eq. (9) until the balance is satisfied within a given tolerance.

### 3.4. Calculation procedure and assumptions

The first law of thermodynamics differentiated in time can be used to calculate the specific internal energy, $u$, with advancement of time $t + \Delta t$ from parameters calculated at the time step $t$:

$$u_1^{t+\Delta t} = (m_1^t u_1^t + \Delta t \left[k_{int}^t A_{int}\left(T_{w\,(int)} - T_1\right)^t - h_1^t \dot{m}_3^t\right])/m_1^{t+\Delta t}, \quad (10)$$

where: $m_1^{t+\Delta t} = m_1^t - \dot{m}_3^t \Delta t.$ (11)

Parameters needed for determination of $k_{int}^t$, i.e., the thermal expansion coefficient $\beta$, dynamic viscosity of the gas $\mu_g$, thermal conductivity of the gas $\lambda_g$, and specific heat at constant pressure $c_{p,g}$, are provided by CoolProp database for $T_1^t$ and $P_1^t$. This allows to calculate $u_1^{t+\Delta t}$. The density of hydrogen in the tank at the time $t + \Delta t$ is calculated as:

$$\rho_1^{t+\Delta t} = \frac{m_1^{t+\Delta t}}{V_{tank}}. \quad (12)$$

Now $u_1^{t+\Delta t}$ and $\rho_1^{t+\Delta t}$ can be used as input to CoolProp database to determine the thermodynamic state of hydrogen at the time $t + \Delta t$: $T_1^{t+\Delta t}$, $P_1^{t+\Delta t}$, $h_1^{t+\Delta t}$. Sections 3.1 and 3.3 describe how to calculate the temperature at the internal tank wall, $T_{w\,(int)}$, and mass flow rate of hydrogen, $\dot{m}_3^t$. The entire calculation algorithm is shown in Table 2 and is implemented in MATLAB [24], with inclusion of open source C++ library CoolProp, implementing NIST EoS [13] and transport properties for hydrogen [18].

Table 2. Calculation algorithm of the non-adiabatic blowdown model including heat transfer through the pipe wall and NIST EoS.

| Step | Calculation algorithm until $P_1/P_{amb}>P_{lim}$* |
|---|---|
| 1 | Hydrogen mass in the tank |
| 2 | Convective heat transfer in the hydrogen tank (Section 3.1) |
| 3 | Change of internal energy to find storage parameters at time $t+\Delta t$ (Section 3.4) |
| 4 | Temperature distribution through the tank wall (Section 3.1) |
| 5 | Heat transfer rate through the discharge pipe wall (Section 3.2) |
| 6 | Real and notional nozzle exits parameters (Section 3.3) |

Note: * - $P_{lim}$ is a limit pressure applied to stop the algorithm calculations. In the present case $P_{lim}$ is taken as 0.3% more than $P_{amb}$.

Calculation of the heat transfer through the tank wall requires the knowledge of the heat transfer coefficient at external tank wall. This parameter is assumed to be constant and equal to 6 W/m$^2$/K for air at ambient temperature [21]. In the cryogenic tests, the stainless-steel tank is immersed in a $LN_2$ bath and the corresponding external heat transfer coefficient is considered to be equal to 120 W/m$^2$/K [25]. The same authors reported a value of 245 W/m$^2$/K for nucleate boiling regime. The assessment of the effect of variation of this value for Test 22c did not demonstrate any significant difference in results. The wall thickness was considered to be uniform throughout the tank and equal to 30 mm, as per the tank walls with largest surface exposed to external conditions. The tank wall is made of stainless steel 1.4571. The properties for the material for the ambient temperature tests are: density $\rho_w$=8000 kg/m$^3$ [26], specific heat $c_{p,w}$=500 J/kg/K [27] and thermal conductivity $\lambda_w$=16.3 W/m/K [28]. The stainless-steel specific heat and thermal conductivity decrease with the temperature. For the cryogenic test the material properties at 80 K are: $c_{p,w}$=200 J/kg/K [29,30] and $\lambda_w$=9.0 W/m/K [29]. The pipe wall temperature at time t=0 s, when solving Eq. (5), is taken from the experiment. The solution of the 1D heat conduction equation for the discharge pipe wall with thickness of 1 mm requires a low time step to satisfy the limit condition in [10]. Even considering just 5 nodes across the pipe wall, a time step lower than 0.004 s would be required. A comparison between transient resolution of temperature across the pipe wall and the simple case with constant temperature $T_w$=222.9 K at the discharge pipe wall for Test 8c, resulted in a maximum variation in calculated mass flow rate of about 5% up to 15 s, but reduction

of calculation time by about 10 times. This difference in calculations is considered to be acceptable and the assumption of constant temperature at the pipe wall equal to experimental measurement at the time 0 s will be accepted in calculations. Nevertheless, for different release geometries and scenarios a transient solution of temperature across the discharge pipe wall shall be considered to obtain accurate estimations. A discharge coefficient, $C_d$, is applied to account for friction and minor losses in the system. The solution of the non-adiabatic blowdown transient, Eqs. (10-12), uses a time step in the range $\Delta t$=0.01-0.05 s depending on the test initial conditions and expected blowdown time. For the tests with larger nozzle diameter ($d_n$=2-4 mm) expecting a blowdown time below 10 s, a converged solution was found for time step $\Delta t$=0.01 s. For the tests with smaller diameter ($d_n$=0.5-1.0 mm) expecting a blowdown time up to 200 s a time step $\Delta t$=0.05 s is found from the convergence study. A further parameter to be considered is the number of nodes $z$ in the spatial discretization of the tank wall ($\Delta x$). $z$=20 was chosen as a compromise between the accuracy and calculation time to ensure its validity also for longer releases with smaller nozzle diameter. For a wall thickness $L_t$=30 mm, $z$=20 ($\Delta x$=1.5 mm), the condition in [10], $\Delta t \ll \frac{1}{2}\frac{\rho_w c_{p,w}}{\lambda_w}\Delta x^2 \ll 0.276$ *s*, is respected, as the chosen $\Delta t$ varies in the range 0.01-0.05 s. The tolerance $\Delta$ and $\Delta T$ were chosen as $\Delta$=100 J/kg and $\Delta T$=0.001 K, as found to be a good compromise between solution accuracy and calculation time. It should be noted that the optimum combination of parameters depends on the specific problem.

## 4. RESULTS AND DISCUSSION

The developed non-adiabatic model for CcH2 provides as output the dynamics of the following quantities during the blowdown of hydrogen from a storage tank: temperature, pressure and density in the tank; mass flow rate; temperature, pressure, density and velocity of hydrogen at the real nozzle exit. The calculations of temperature and pressure dynamics inside the storage tank by the physical model are validated against experimental data. The discharge coefficient, $C_d$, is applied in calculations to account for friction and minor losses in the piping system and real nozzle compared to the ideal case of no losses with $C_d$=1. For each of the simulated tests, different discharge coefficients are applied to find the optimum characteristic for this experiment. Figure 3 compares pressure and temperature dynamics for eight tests at cryogenic temperature. The calculated temperature is compared with experimental temperature, TCave, averaged arithmetically over the readings of three type K "closed" thermocouples (i.e., with a stainless-steel sensitive tip) located at different heights in the tank. The developed model reproduces well the experimental pressure and temperature dynamics for all these tests. The arithmetical averaging of the three experimental temperature readings, TCave, instead of mass-averaging may be a cause of the generally slight deviation of TCave from the calculated temperature in the storage tank. Tests 16c and 22c with the largest diameter ($d_n$=4.0 mm) result in somewhat lower temperature compared to the experimental one. This may be associated with the inertia of the "closed" thermocouples, which may not well capture the steeper variation of temperature associated with these faster blowdowns and the possible corresponding higher gas flow speed. A deeper analysis of this issue will be carried out in Section 4.1. Tests 16c and 22c show a larger deviation among the records of the three thermocouples inside the tank, signalling a larger non-uniformity of temperature distribution within the tank. Tests with lower initial storage pressure (about 0.6 MPa abs) present a certain level of noise when approaching the ambient pressure, whereas as expected calculations tend to zero. The optimum discharge coefficients for the whole set of tests are found to be in the range $C_d$=0.6-0.8. The maximum calculated hydrogen mass flow rate is at the start of blowdown (defines the time step $\Delta t$) and varies greatly from 0.1 to 6.6 g/s when increasing diameter from 0.5 to 4.0 mm for an initial storage pressure of 0.6 MPa abs. For tests with initial storage pressure of about 20 MPa abs, the hydrogen mass flow rate varies in the range 4.3-241.7 g/s. The calculation time on a quad-core laptop varies from 15 min to 19 hours depending on the test initial pressure and nozzle diameter.

Figure 4 shows the comparison of calculations against experiments with initial storage temperature equal to ambient and nozzle diameter equal to 0.5 and 4.0 mm. The comparison confirms the accurate predictive capability of the developed non-adiabatic blowdown model. Similar observations as per cryogenic tests can be made for Test 16w and Test 22w with shortest blowdown time (see Section 4.1 for details). The optimum discharge coefficient for all the set of ambient temperature tests is in the same range $C_d$=0.6-0.8 as for cryogenic temperatures. The calculated hydrogen mass flow rate varies in the

range 0.049-2.8 g/s for initial storage pressure of 0.6 MPa abs, whereas it varies in the range 1.9-107.0 g/s for pressure of 20 MPa abs.

| Case | Overpressure dynamics | Temperature dynamics |
|---|---|---|
| Test 1c - $P_1$=0.59 MPa abs, $T_1$=83.7 K, $d_n$=0.5 mm | 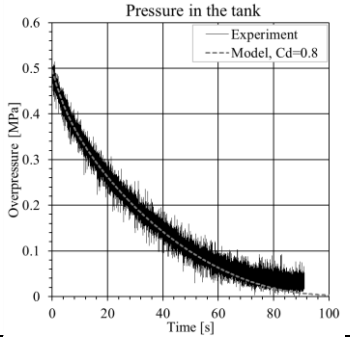 | 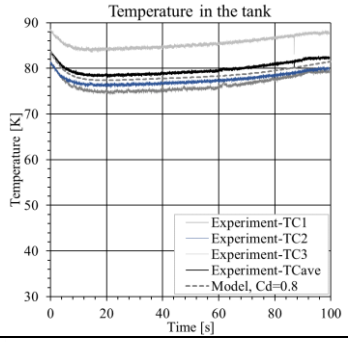 |
| Test 4c - $P_1$=20.12 MPa abs, $T_1$=80.2 K, $d_n$=0.5 mm | 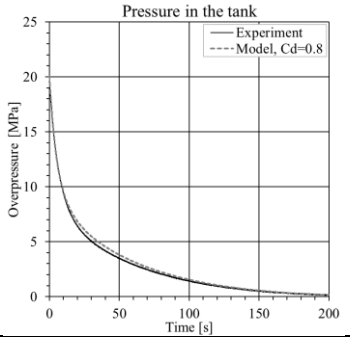 | 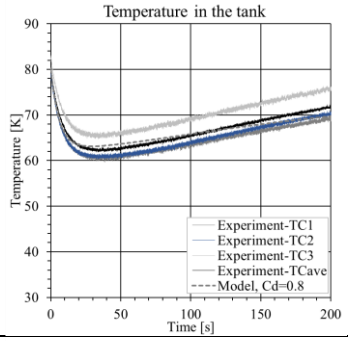 |
| Test 5c - $P_1$=0.61 MPa abs, $T_1$=86.0 K, $d_n$=1.0 mm | 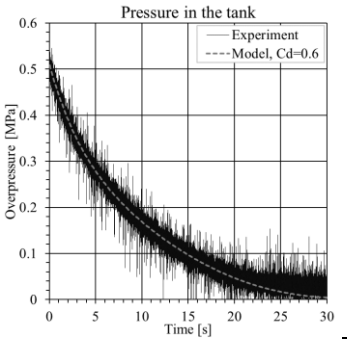 | 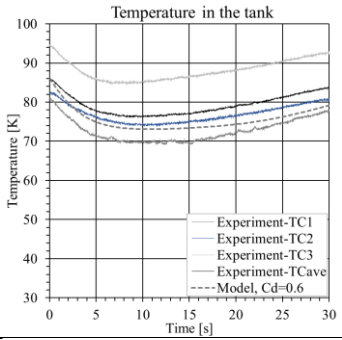 |
| Test 8c - $P_1$=20.10 MPa abs, $T_1$=84.8 K, $d_n$=1.0 mm | 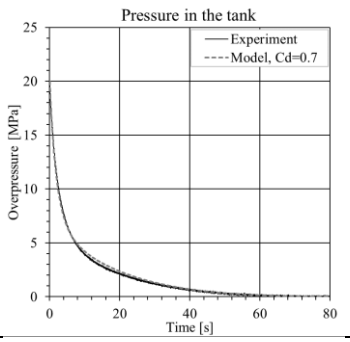 | 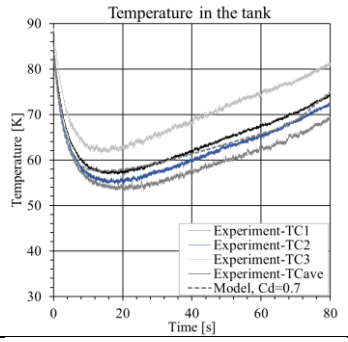 |
| Test 9c - $P_1$=0.60 MPa abs, $T_1$=81.2 K, $d_n$=2.0 mm | 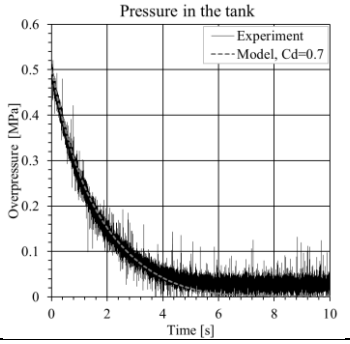 | 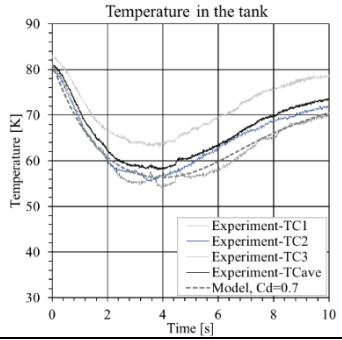 |

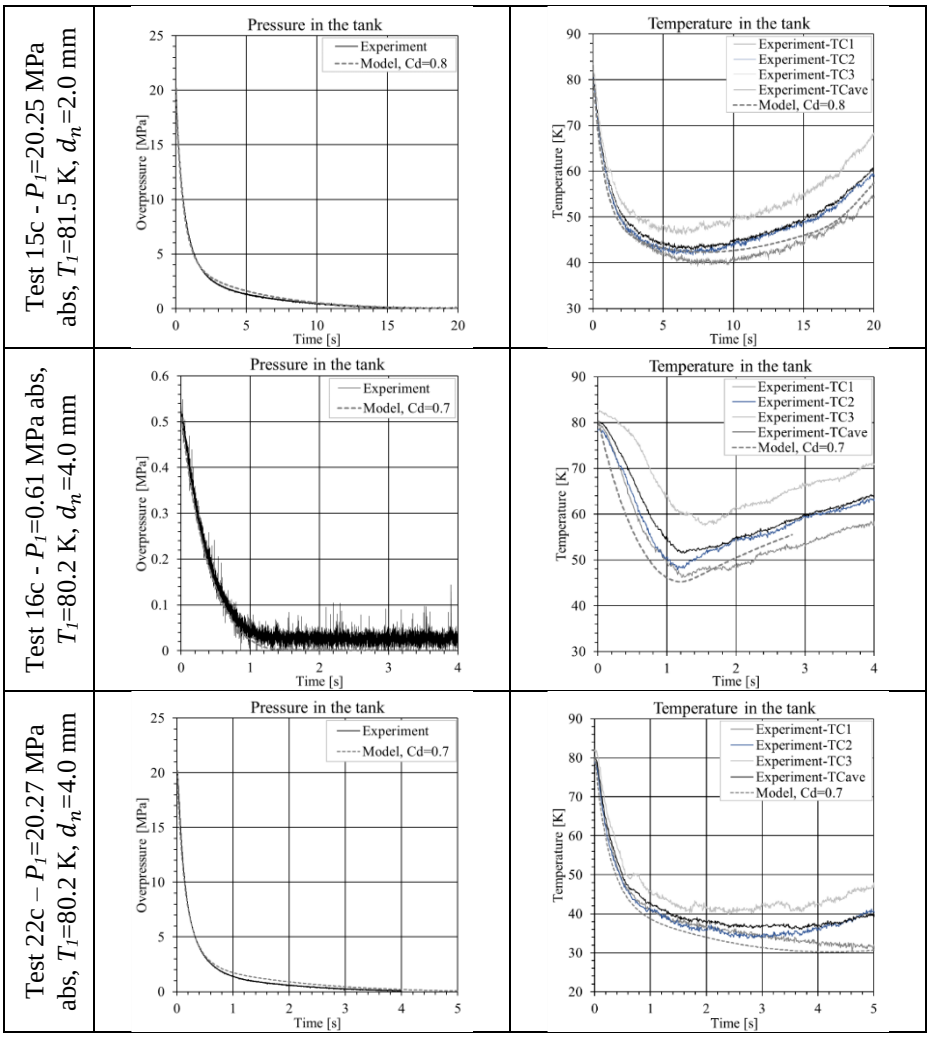


Figure 3. Validation of the developed non-adiabatic blowdown model against experiments at initial cryogenic temperature.

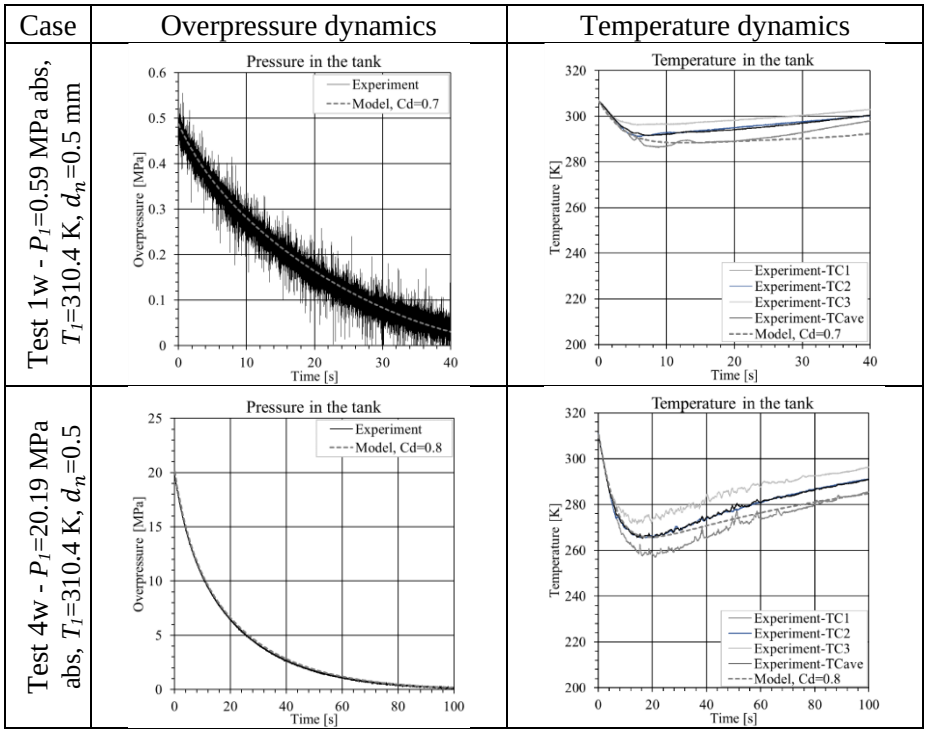

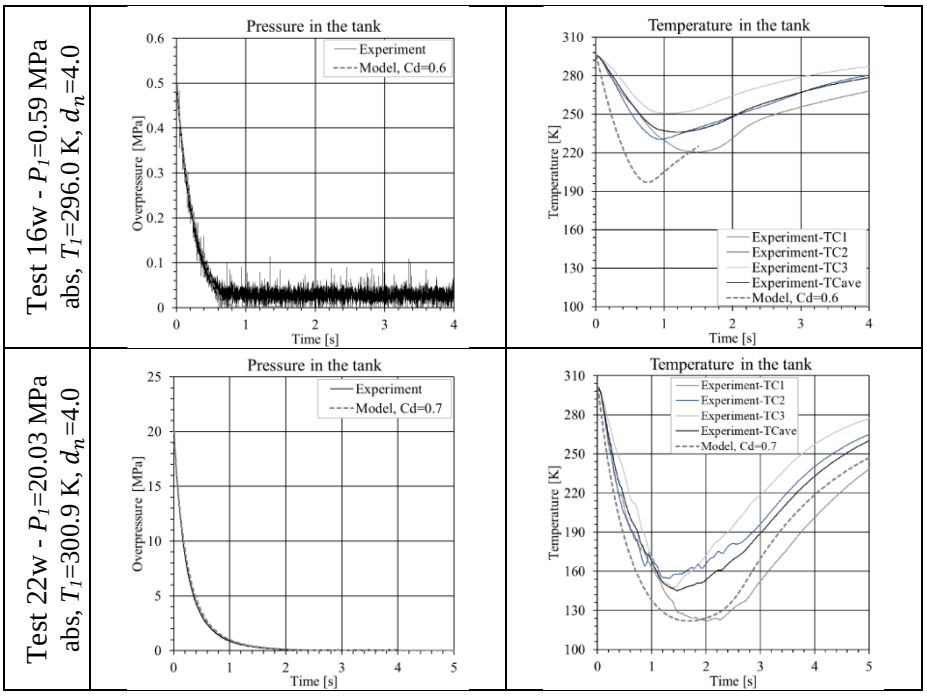


Figure 4. Validation of the developed non-adiabatic blowdown model against experiments at initial ambient temperature.

### 4.1. The effect of thermocouple inertia

Predictions of pressure and temperature dynamics in the storage tank are seen to agree well with experimental measurements. Few exceptions are given by the releases with larger diameter, e.g. Test 16w ($P_1$=0.59 MPa abs, $T_1$=296.0 K, $d_n$=4.0 mm). This deviation is deemed to be caused by the thermocouple inertia being comparable with the blowdown duration. Indeed, Test 16w is one of the tests showing the largest difference in temperature measurements by the "closed" and "open" type of thermocouples, both used in this experiment conversely to other tests. "Open" thermocouples had the stainless-steel tip removed, decreasing the thermocouple inertia but as well reducing measurements accuracy for cryogenic temperatures [20]. Figure 5 shows the comparison between the predicted temperature in the storage tank and experimental measurements by the two thermocouple types. The "open" thermocouples measurements give better agreement with the model calculations due to reduced sensors inertia. This is important for such a short blowdown duration. However, these sensors may lose accuracy for reduced temperatures, including cryogenic, and thus "closed" thermocouples were used in the experiments and thus in the model validation process.

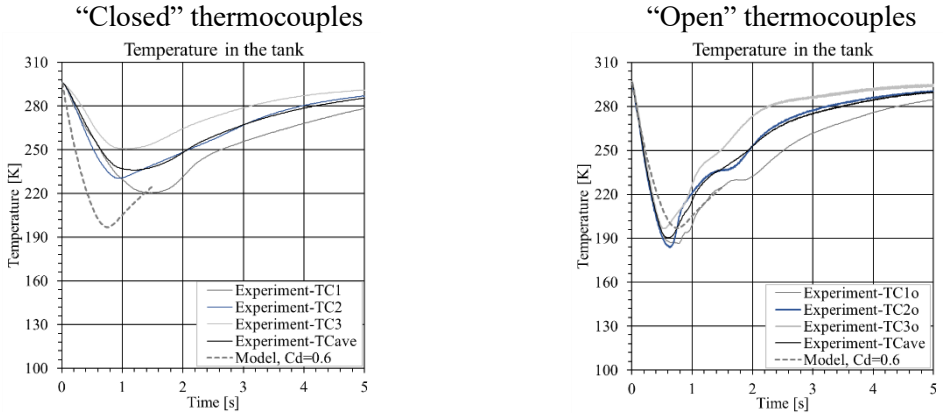


Figure 5. Storage temperature dynamics for Test 16w ($P_1$=0.59 MPa abs, $T_1$=296.0 K, $d_n$=4.0 mm): "closed" versus "open" thermocouples' experimental measurements.

## 5. CONCLUSIONS

The ***originality*** of this study is in the development of the physical model accounting for the effect of conjugate heat transfer through the storage tank and discharge pipe walls. The non-ideal behaviour of hydrogen at cryogenic temperatures and high pressures is accounted for by using the NIST EoS and CoolProp properties database.

The ***significance*** of the work is in the provision of a validated physical model to predict accurately the dynamics and characteristics of transient cryo-compressed hydrogen releases during storage tank blowdown. A proper calculation of parameters at the real nozzle through the validated physical model allows to simulate accurately the dispersion of hydrogen jet and thus properly assess hazard distances.

The ***rigour*** of this study is given by the extensive validation against sixteen experiments performed within the PRESLHY project at initial ambient and cryogenic (80 K) temperatures. The initial storage pressure was in the range 0.6-20 MPa abs, whereas the release diameter varied from 0.5 mm to 4.0 mm. The model reproduced well the experimentally measured pressure and temperature dynamics inside the tank during blowdown experiments. The difference between calculations and experiments was within the accuracy of experimental measurements and comparable to the deviation between the recordings of the three thermocouples placed inside the tank at difference heights. Somewhat larger differences between calculations and experiments were observed for the tests with larger release diameters of 2 mm and 4 mm. This is shown to be associated with the thermocouples inertia. Further research is envisaged to progress towards the assessment of the validation and applicability of the developed physical model to larger hydrogen storages, full bore ruptures and longer discharge lines once detailed experiments will be available.

## ACKNOWLEDGEMENTS

This research has received funding from the Fuel Cells and Hydrogen 2 Joint Undertaking (now Clean Hydrogen Partnership) under grant agreement No.779613 (PRESLHY), No.826193 (HyTunnel-CS), No.875089 (HyResponder) and No. 101101381 (ELVHYS). ELVHYS project is supported by the Clean Hydrogen Partnership and its members. UK participants in Horizon Europe Project ELVHYS are supported by UKRI grant numbers 10063519 (University of Ulster) and 10070592 (Health and Safety Executive).
Disclaimer: Funded by the European Union. Views and opinions expressed are however those of the authors only and do not necessarily reflect those of the European Union or the Clean Hydrogen Partnership. Neither the European Union nor the Clean Hydrogen Partnership can be held responsible for them.

## REFERENCES

[1] DOE. Technical Assessment: Cryo-Compressed Hydrogen Storage for Vehicular Applications. 2006.

[2] Stetson NT, McWhorter S, Ahn CC. Introduction to hydrogen storage. In: Gupta RB, Basile A, Veziroğlu TN, editors. Compend. Hydrog. Energy, Woodhead Publishing; 2016, p. 3–25.

[3] Aceves SM, Berry GD, Rambach GD. Insulated pressure vessels for hydrogen storage on vehicles. Int J Hydrogen Energy 1998;23:583–91. https://doi.org/10.1016/s0360-3199(97)00079-7.

[4] Petitpas G, Bénard P, Klebanoff LE, Xiao J, Aceves S. A comparative analysis of the cryo-compression and cryo-adsorption hydrogen storage methods. Int J Hydrogen Energy 2014;39:10564–84. https://doi.org/10.1016/j.ijhydene.2014.04.200.

[5] Brunner T. BMW Hydrogen . Hydrogen Storage Workshop. Cryo-compressed Hydrogen Storage., Washington D.C: 2011.

[6] Schefer RW, Houf WG, Williams TC, Bourne B, Colton J. Characterization of high-pressure, underexpanded hydrogen-jet flames. Int J Hydrogen Energy 2007;32:2081–93.

[7] Monde M, Mitsutake Y, Woodfield PL, Maruyama S. Characteristics of Heat Transfer and Temperature Rise of Hydrogen during Rapid Hydrogen Filling at High Pressure 2007;36:13–27.

[8] Woodfield PL, Monde M, Takano T. Heat Transfer Characteristics for Practical Hydrogen Pressure Vessels Being Filled at High Pressure. J Therm Sci Technol 2008;3:241–53.

[9] Monde M, Woodfield P, Takano T, Kosaka M. Estimation of temperature change in practical hydrogen pressure tanks being filled at high pressures of 35 and 70 MPa. Int J Hydrogen Energy 2012;37:5723–34. https://doi.org/10.1016/j.ijhydene.2011.12.136.

[10] Molkov V, Dadashzadeh M, Makarov D. Physical model of onboard hydrogen storage tank thermal behaviour during fuelling. Int J Hydrogen Energy 2019;44:4374–84.

[11] Molkov V, Dadashzadeh M, Kashkarov S, Makarov D. Performance of hydrogen storage tank with TPRD in an engulfing fire. Int J Hydrog Energy 2021;46:36581–97.

[12] Molkov V, Makarov V, Bragin M V. Physics and modelling of underexpanded jets and hydrogen dispersion in atmosphere. Phys Extrem States Matter 2009:146–9.

[13] Leachman JW, Jacobsen RT, Penoncello SG, Lemmon EW. Fundamental equations of state for parahydrogen, normal hydrogen, and orthohydrogen. J Phys Chem Ref Data 2009.

[14] Cirrone D, Makarov D, Molkov V. Thermal radiation from cryogenic hydrogen jet fires. Int J Hydrogen Energy 2019;44:8874–85. https://doi.org/10.1016/j.ijhydene.2018.08.107.

[15] Cirrone D, Makarov D, Molkov V. Cryogenic hydrogen jets: flammable envelope size and hazard distances for jet fire. Int. Conf. Hydrog. Saf., Adelaide, Australia: 2019.

[16] Cirrone D, Makarov D, Kuznetsov M, Friedrich A, Molkov V. Effect of heat transfer through the release pipe on simulations of cryogenic hydrogen jet fires and hazard distances. Int J Hydrogen Energy 2022;47:21596–611. https://doi.org/10.1016/j.ijhydene.2022.04.276.

[17] Venetsanos AG, Giannissi S, Tolias I, Friedrich A, Kuznetsov M, Gmbh P. Cryogenic and ambient gaseous hydrogen blowdown with discharge line effects. ID178. Int. Conf. Hydrog. Saf., Edinburgh, Scotland, UK: 2021, p. 1–11.

[18] Bell IH, Wronski J, Quoilin S, Lemort V. Pure and Pseudo-pure Fluid Thermophysical Property Evaluation and the Open-Source Thermophysical Property Library CoolProp. Ind Eng Chem Res 2014;53:2498–508.

[19] Friedrich A, Veser A, Jordan T. PRESLHY - D3.4 Summary of experiment series E3.1 (Discharge) results. 2019.

[20] Veser A, Friedrich A, Kuznetsov M, Jordan T, Kotchourko N. Hydrogen blowdown release experiments at different temperatures in the discha-facility. ID38. 9th Int. Conf. Hydrog. Safety, 21st-24th Sept. 2021, Edinburgh, UK: 2021, p. 442–54.

[21] Dadashzadeh M, Makarov D, Kashkarov S, Molkov V. Non-adiabatic under-expanded jet theory for blowdown and fire resistance rating of hydrogen. Int. Conf. Hydrog. Saf., Adelaide, Australia: 2019.

[22] Patankar S. Numerical Heat Transfer and Fluid Flow: Computational Methods in Mechanics and Thermal Science. 1980.

[23] The Engineering Toolbox. Heating Up Applications - Energy Required and Heat Transfer Rates 2022. https://www.engineeringtoolbox.com/heat-up-energy-d_1055.html.

[24] The Mathworks Inc. MATLAB: R2021a 2021.

[25] Wang T, Zhao G, Tang H, Jiang Z. Determination of convective heat transfer coefficient at the outer surface of a cryovial being plunged into liquid nitrogen. Cryo-Letters 2015;36:285–8.

[26] MatWeb. Material property data. 316 Stainless Steel, annealed bar 2021. https://www.matweb.com

[27] Thyssenkrupp. Stainless Steel 316Ti 1.4571 2021. https://www.thyssenkrupp-materials.co.uk/stainless-steel-316ti-14571.html.

[28] Aalco Metals Ltd. Stainless Steel 1.4571 - 316T 2021. http://www-eng.lbl.gov/~shuman/NEXT/MATERIALS%26COMPONENTS/Pressure_vessels/Aalco-Metals-Ltd_Stainless-Steel_1.4571-316Ti_40.pdf.

[29] Polinski J. Materials in cryogenics Content. Eur Course Cryog 2010.

[30] Duthil P. Material properties at low temperature. CAS-CERN Accel Sch Supercond Accel - Proc 2014;005:77–95. https://doi.org/10.5170/CERN-2014-005.77.